CFD Letters

Aerodynamic Design and Modeling of Large-Scale Offshore Wind Turbines

Open Access

Auraluck Pichitkul[1,*], Lakshmi N Sankar[1]

[1] School of Aerospace Engineering, Georgia Institute of Technology, United States of America

ARTICLE INFO	ABSTRACT
	A large-scale offshore 2 MW wind turbine designed to operate in a proposed 120-MW North Sea windfarm project is investigated in this study. The wind resources at the proposed site and the power requirements of the wind farm have been established. Preliminary sizing and conceptual design of a 2 MW wind turbine has been carried out to achieve optimum aerodynamic performance. Aerodynamic performance of the proposed design has been independently analysed by classical blade element-momentum (BEM) theory and by an in-house computational fluid dynamics (CFD) analysis. The CFD analysis has in the past been used only for small scale 10KW class turbines and required a distributed computing platform. As part of the work, this approach has been extended to large-scale wind turbine systems, and implemented in a form suitable for efficient execution on modern multi-core desktop systems with the aid of message passing interface (MPI). The tip vortex model in earlier hybrid analyses has been extended to incorporate a full span wake model. In the event of unsteady stalled flow over the rotor at high wind speeds, the present approach also captures the shed wake effects. The results from both the BEM and CFD analyses agree well with each other in terms of performance. It is found that the proposed design is efficient in terms of power generation over a broad range of wind speeds, tip speed ratios, and blade pitch settings with a maximum coefficient of power around 0.47. An economic feasibility study of the proposed offshore windfarm has also been done. The cost of energy was found to be 9.7 cents per KW-hr in 2018 dollars, which is significantly lower than the prevailing cost of 18 cents per KW-hr. It is concluded that the windfarm project is economically viable.

1. Introduction

Carbon dioxide and greenhouse gas emission has recently become an important environmental concern around the world. Numerous efforts are being made by governments worldwide, to reduce fossil fuel consumption and rely more on renewable energy resources. Among renewable energy alternatives, wind energy is one of the most prevalent and popular. The abundance of wind resources

---

Corresponding author.
E-mail address: apichitkul3@gatech.edu (Auraluck Pichitkul)

worldwide, combined with rapid advancements in wind engineering technology, has made wind energy a very promising renewable energy option.

Over the past several decades, extensive research has been carried in this field to model the physics of wind turbine operations efficiently and accurately, and on improving turbine performance and efficiency. Much of the early work in this area relied on field studies where the wind turbine performance was measured at various wind speeds. National Renewable Energy Laboratory (NREL) in the United States has measured and documented the performance of a number of rotor systems. These include field studies as well as carefully done wind tunnel studies [1-5]. Efficient computational methods that use blade element theory for the aerodynamics of the rotor blades, combined with conservation of axial and azimuthal momentum within an annulus stream tube crossing the rotor disk (BEM) also became available [6-8]. With the routine availability of highspeed computer systems, efficient computational fluid dynamics (CFD) methodologies also became available [9-21].

Coupling of wind turbines with other disciplines such as aeroelasticity and wind drive trains have also been done. In Yu *et al.,* [22]'s study, a 3-dimensional unstructured grid methodology was coupled to a flexible beam model. In Becker *et al.,* [23]'s research, the NREL public domain software FAST [24] has been coupled to the open source software OpenFoam [25] to model the effects of blade bending and torsional effects, and the drive train inertia. In Popko *et al.,* [26]'s analysis, validation and comparison of various aerodynamics-hydrodynamics-servo-elastics simulation codes for offshore wind turbines have been made.

In the present study, these advances in computational modeling of wind turbines are used to conduct a feasibility study of a hypothetical windfarm. This farm consists of 60 wind turbines, each producing 2 MW of power for a total power production of 120 MW. The proposed farm is located in the North Sea region on the west side of the West Frisian Islands off the coast of the Netherlands. This region is rich in wind resources [27-29] as shown in Figure 1.
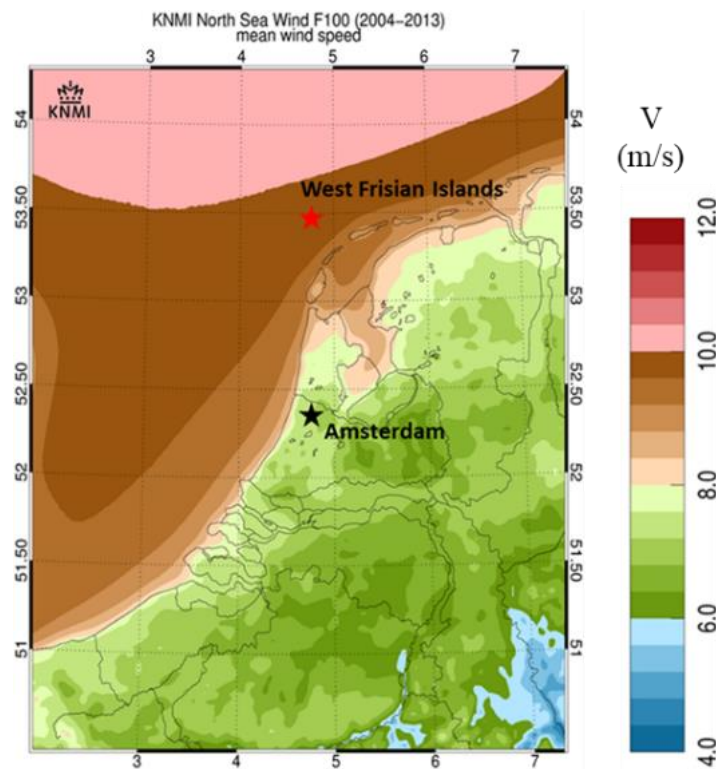

Fig. 1. Wind map in North Sea region [27]

2. Methodology

In this work, the proposed windfarm modelled using the following approach. First, the combined blade element-momentum theory (BEM) has been used to design a wind turbine with a rated power of 2 MW at a rated wind speed of 10 m/s. The aerodynamic performance of the wind turbine is subsequently analyzed at off design conditions using BEM theory. These numerical predictions are independently verified using a state-of-the-art computational fluid dynamics solver developed by the present authors at selected operating conditions. Finally, an economic feasibility study is done to assess the economic viability of the proposed windfarm.

2.1 Wind Turbine Blade Design

As previously described, the wind turbine is designed for the following operating conditions

i.   Rated power: 2 MW
ii. Rated wind speed: 10 m/s
iii. Site elevation: 0 m
iv. Air density 1.225 kg/m3

2.1.1 Preliminary sizing

The design process begins with the selection of the number of blades. For large-scale wind turbines, a 3-bladed configuration is common [30]. Assuming a rated wind speed of 12 m/s at the hub of the rotor disk (120% of the prevailing wind speed at sea level), and a nominal power coefficient C_P of 0.5, we obtain a preliminary estimate of the blade radius R from

$$P = \frac{1}{2}\rho C_P \pi R^2 V_{hub}^3 \tag{1}$$

The hub height is next determined to be twice the blade radius R, based on NREL Wind Pact Trade Studies [23].

$$h_{hub} = 2R \tag{2}$$

We next use the rated wind speed at a specified anemometer height to project the wind speed at the center of the rotor hub using the 1/7 power law for turbulent boundary layers:

$$V_{hub} = V_{anemometer}\left(\frac{h_{hub}}{h_{anemometer}}\right)^{\frac{1}{7}} = V_{anemometer}\left(\frac{2R}{h_{anemometer}}\right)^{\frac{1}{7}} \tag{3}$$

Eq. 1 - 3 are iteratively solved until the bade radius R converges to a user specified tolerance. For the proposed wind turbine, the rotor radius is found to be 46.34 m.

The next design parameter to be considered is the rotor revolutions per minute (RPM). Based on historical data and previous analyses [30], the optimum value of tip speed ratio (TSR), defined as the ratio of the tip speed to the velocity at the hub, generally varies between 10 and 12. A nominal TSR of 11, corresponding to an RPM of 22.5, has been selected.

2.1.2 Airfoil selection

Following the guidelines from Tangler *et al.,* [31]'s study, NREL airfoil families of S818, S825, and S826 are used at the blade root, mid-span, and tip section, respectively as shown in Table 1 below. These airfoils are well known for their high values of maximum lift coefficient, gradual progressive stall, and laminar flow with low viscous drag over a broad range of angles of attack. These air-foils are also insensitive to roughness due to grid, ice, or erosion of the blade surface.

Table 1
Airfoil Families used in the Proposed Design

r/R	Airfoil	Thickness
$0.05 \leq r/R \leq 0.45$	S818	24%
$0.45 < r/R \leq 0.85$	S825	17%
$0.85 < r/R \leq 1.00$	S826	14%

2.1.3 Blade twist

The radial distribution of blade twist is next found as follows in Figure 2.
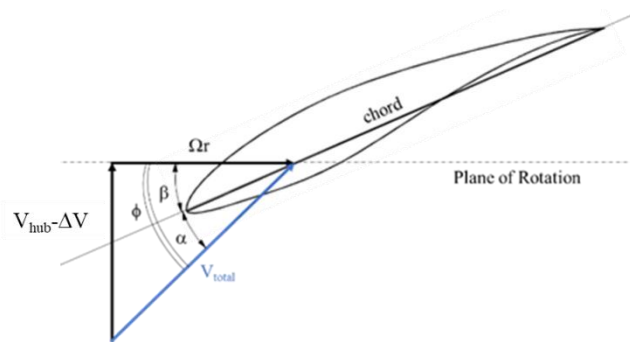

Fig. 2. Schematic diagram of local blade section and the corresponding flow angles

Here, the quantity ΔV is the induced velocity. According to Betz theory for actuator disks, ΔV should be $V_{hub}/3$ for maximum efficiency.

From Figure 2 above, the twist angle β for zero pitch operation is given by

$$\beta = \phi - \alpha \qquad (4)$$

The local flow angle ϕ is given by

$$\phi = tan^{-1}\left(\frac{V_N}{V_T}\right) \approx tan^{-1}\left(\frac{2}{3}\frac{V_{hub}}{\Omega r}\right) \qquad (5)$$

The angle of attack α in Eq. 4 above corresponds to an angle of attack that yields the maximum lift-to-drag ratio for a given airfoil shape. The factor 2/3 in Eq. 5 is based on Betz actuator disk model, which states that the optimum performance is realized when the wind speed slows down to 2/3 of its value far upstream of the rotor disk. Eq. 4 and 5 result in a nonlinear twist distribution in the radial direction along the blade. In the present study, a linear regression of the blade twist distribution was done to arrive at a configuration that is easily manufactured.

2.1.4 Blade chord selection

The next step is to determine radial distribution of chord length. According to BEM theory, air particles that cross an annular ring of radius r and width Δr experience a rate of change of momentum caused by the aerodynamic forces exerted by the blade sections on the particles:

$$\rho(2\pi r \Delta r)(V_{hub} - \Delta V)(2\Delta V) = B(L^{'} \cos\phi + D^{'} \sin\phi)\Delta r \tag{6}$$

Again, ΔV is $V_{hub}/3$ based on the Betz actuator model for optimum performance. The air particles continue to decelerate behind the rotor disk and far field downstream, so that the total change in the velocity between a station far upstream and a station far downstream is $2\Delta V$.

Here L' and D' are the lift and drag forces on the blade section per unit span. Using the definition of these aerodynamic forces in Eq. 6, we obtain

$$\frac{16}{9}\pi r V_{hub}^2 = \left[\frac{B}{2}\left(\frac{4}{9}V_{hub}^2 + (\Omega r)^2\right)c\right](c_l \cos\phi + c_d \sin\phi) \tag{7}$$

The blade chord c(r) may be found from Eq. 7. A linear regression of the chord variation is next done, in order to arrive at a trapezoidal blade planform as shown in Figure 3.
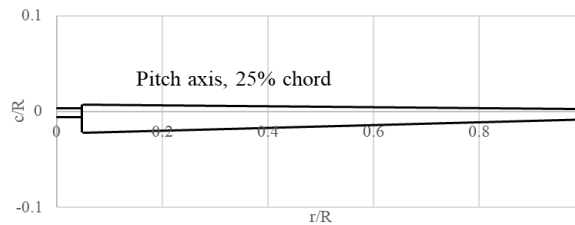

Fig. 3. Geometry of rotor blade planform

2.1.5 Rotor design summary

From the design procedure discussed earlier, the final design of the proposed wind turbine is summarized in Table 2 below

Table 2
Summary of Rotor Design

Design Parameter	Value
Number of Blades, B	3
Rated Power (MW)	2
Rated Wind Speed (m/s)	10
Rotor Radius (m)	46.34
Hub Height (m)	92.68
Design RPM	22.5
Rated Tip Speed (m/s)	109.2
Rated Tip Speed Ratio (TSR)	10.92
Root Cut-out	5% Radius
Airfoil Families	Root: S818
	Mid Span: S825
	Tip: S826

2.2 Preliminary Performance Analysis by BEM

Primary investigation of wind turbine performance under design and off-design conditions is conducted using classical combined blade element momentum (BEM) theory. The reference rotor blade is divided radially into a number of blade elements. Each of the blade elements is then aerodynamically analysed as a two-dimensional flow problem. Referring to a schematic diagram of the problem described by Figure 4, BEM theory computes aerodynamic loads using the following procedure.
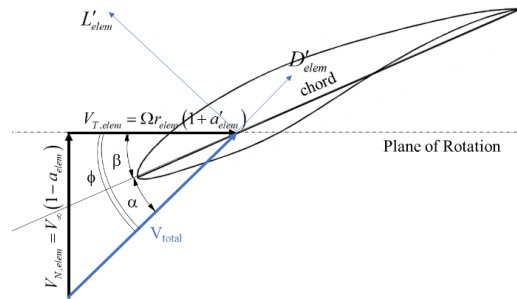

Fig. 4. Schematic diagram of velocity and force components of a blade element located at a radial distance r from the center of rotation

For each element, an initial guess is made for axial induction factor, and rotational factor, using Eq. 8 and 9 given below.

$$a_{guess} = \frac{1}{4}\left[2 + \pi\lambda_{elem}\sigma_{elem} - \sqrt{4 - 4\pi\lambda_{elem}\sigma_{elem} + \pi\lambda_{elem}^2\sigma_{elem}(8\beta_{elem} + \pi\sigma_{elem})}\right] \tag{8}$$

$$a'_{guess} = 0 \tag{9}$$

where

$$\beta_{elem} = twist_{elem} + pitc\square$$

$$\lambda_{elem} = \frac{\omega r_{elem}}{V_\infty} \ and \ \sigma_{elem} = \frac{Bc_{elem}}{2\pi r_{elem}}$$

$$V_{N,elem} = V_\infty(1 - a_{elem})$$

$$V_{T,elem} = \Omega r_{elem}(1 + a'_{elem})$$

$$\phi_{elem} = arctan\left(\frac{V_N}{V_T}\right)_{elem}$$

$$\alpha_{elem} = \phi_{elem} - \beta_{elem}$$

$$L'_{elem} = \frac{1}{2}\rho_\infty(V_N^2 + V_T^2)_{elem}c_{elem}C_{l,elem}$$

$$D'_{elem} = \frac{1}{2}\rho_\infty(V_N^2 + V_T^2)_{elem}c_{elem}C_{d,elem}$$

Once the lift and drag forces per unit span of an element are obtained, thrust force acting on the element and power produced by the element can be found using Eq. 10 and 11, respectively.

$$T'_{elem} = L'_{elem} \sin\phi_{elem} - D'_{elem} \cos\phi_{elem} \qquad (10)$$

$$P_{elem} = T'_{elem}(\Delta r)\Omega r_{elem} \qquad (11)$$

Total thrust and power produced by the entire rotor can there-fore be obtained by summing thrust and power contributions of each blade element determined by Eq. 10 and 11 over all elements, and multiplying the thrust and power per blade the number of blades, i.e.,

$$T_{total} = B\sum_N T'_{elem} \qquad (12)$$

$$P_{total} = B\sum_N P_{elem} \qquad (13)$$

The earlier estimated values of axial induction factor and the swirl induction factor are updated using Eq. 14 and 15 below.

$$a_{new} = \left[1 + \frac{4F\sin^2\phi_{elem}}{\sigma_{elem}(C_{l,elem}\cos\phi_{elem} + C_{d,elem}\sin\phi_{elem})}\right]^{-1} \qquad (14)$$

$$a'_{new} = \left[-1 + \frac{4F\sin\phi_{elem}\cos\phi_{elem}}{\sigma_{elem}(C_{l,elem}\sin\phi_{elem} - C_{d,elem}\cos\phi_{elem})}\right]^{-1} \qquad (15)$$

Where

$$F = F_{tip}F_{hub}$$

$$F_{tip} = \frac{2}{\pi}arccos\, e^{-\left(\frac{B(R - r_{elem})}{2r_{elem}\sin\phi_{elem}}\right)}$$

Hub losses were neglected. Thus, F_{hub} equals 1. Eq. 8-15 are iteratively updated until a and a' converge to user specified tolerance for all the blade elements.

In the present study, a MATLAB solver based on the above theory has been developed. A root cut out of 5% is assumed. The remaining blade area between 5% R and 100%R is divided equally into 19 blade elements. The BEM code also corrects for azimuthal variation in wind speeds due to ground boundary layer effects.

2.3 Aerodynamic Modelling and Analysis by CFD

In addition to preliminary performance calculations by BEM as previously discussed in 2.2, CFD analysis of the wind turbine rotor has also been conducted to complement BEM results, and visualize important flow features.

2.3.1 CFD methodology: the hybrid method

An in-house CFD solver called GT-Hybrid is used for all cases in this study. GT-Hybrid employs a hybrid approach [10, 20]. It combines a Navier-Stokes solver (RANS) that simulates the viscous flow over the blade in the near field, with a Lagrangian wake representation of the trailing and shed wake structure. Because only a small region surrounding the blades is solved using the costly Navier-Stokes equations, the present hybrid method is computationally very efficient.

A free wake model, which allows for wake distortion, is used to compute wake geometry. Biot-Savart law is used to compute self-induced velocity of the wake, as well as the induced velocity caused by the blade on the computational fluid dynamics region boundaries.

The tip vortex model in our earlier hybrid analyses has been generalized to incorporate a full span wake model to capture the tip vortex as well as the inner wake. In the event of unsteady stalled flow over the rotor at high wind speeds or under cross wind conditions, the present approach also captures the shed wake effects.

The present numerical scheme is first order accurate in time and third order accurate in space. The Spalart-Allmaras Detached Eddy Simulation (SA-DES) is used for modelling the effects of eddy viscosity. This model was chosen from an extensive study of available turbulence models within the flow solver. These include the Baldwin-Lomax algebraic model, SA-DES model, and the classical k-ω-SST two-equation model. In Benjanirat [11]'s research, it was found that the SA-DES model wasadequate for modelling attached and separated flow regimes, both.

As part of the work, the approach in our earlier work [10, 20] has been extended to large scale wind turbine systems and implemented in a form suitable for efficient execution on multi-core desktop systems. The earlier version of the solver required 26 hours on a Pentium IV desktop system for four revolutions. The present analysis takes advantage of improved clock speeds and multiple cores available on modern desktop system and uses the MPI (message passing interface) for a more efficient simulation, requiring less than 2 hours of wall clock system for four revolutions.

2.3.2 Computational grid topology

GT-Hybrid solver package includes a grid generator. For all computational cases, a C-H grid topology is used due to its flexibility in near-surface grid refinement, together with orthogonality and smoothness of grid lines. In the current study, all computational grids are clustered near the leading edge, the trailing edge, and the blade tip, and are created with the following settings (Table 3)

Table 3
Computational grid settings

Parameter	Value
Number of wrap-around-chord grid lines	131
Number of grid lines above/below blade surface	45
Number of grid lines in spanwise direction	70
Associated y+ value	5

Grid sensitivity studies have been done in prior work [10] where three progressively refined meshes ranging from 600,000 cells to 2.4 Million cells per blade were studied, and the sectional thrust coefficient and the power coefficient both varied within 5%. For engineering analyses, the grid density shown in Table 3 has been found to be adequate.

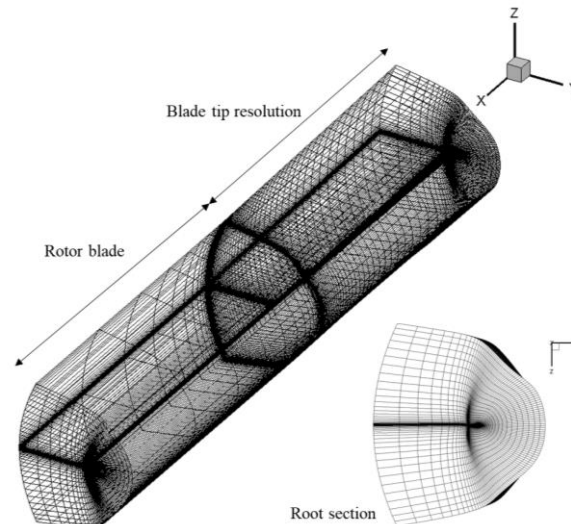An illustration of computational grid used in this study is given below in Figure 5.

Fig. 5. Computational grid used in the current study

2.4 Cost of Energy

An economic analysis has been carried out for the proposed wind form, using a cost model proposed in Wijnent [27]'s analysis as follows.

First, a Weibull probability distribution PWeibull(V) of the wind speed at the proposed site is assumed. Nest, the power production at a given wind speed is computed as P(V) from Eq. 1. The product of P(V) times $P_{Weibull}$(V) is numerically integrated between the cut-in speed and cut-out speeds. This integral yields the estimated power per wind turbine. Multiplying this value by the number days (365) and hours per day (24), the total annual energy production in KW-hours is computed.

For the proposed wind turbine configuration, this approach indicates that the offshore windfarm will have a capacity factor of 52.87%, with an annual energy production of 9262 MW-hr.

Next, the total cost of the wind turbine was estimated using the cost model given in previous study [32]. In this model, regression curve fit data is used for the estimated cost of the various components – rotor blades, gears, tower, nacelle, support systems, etc. The costs associated with offshore systems were also included. This approach projects that the initial cost of a 2 MW offshore system is3.6 Million in 2002 US dollars.

Once the capital cost is known, the annual cost of servicing this debt may be estimated as follows. The cost is met using a combination of equity (with an anticipated 15% return on equity) and commercial bank loans (at 8.7%) for an average rate of 11.85%. The financing cost per year divided by the total annual energy production (9.3 GW-hr for this site) yields a value of 5.1 US cents per KW-hr as the cost of energy in 2002 dollars, after the annual cost of maintenance, repair, and overhaul (MRO) are considered.

This value, adjusted for inflation of 2%, is 9.7 US cents per Kilowatt-hour in 2018 dollars. This amount is substantially lower than the utility rate of 18 cents per KW-hr in Netherlands, indicating that the proposed wind form is financially viable.

3. Results and Discussion

For both BEM and CFD investigations, aerodynamic performance of the wind turbine design is assessed for the following cases

i. Wind speed: 6-25 m/s
ii. Pitch angle: 0 deg, 2 deg, and 4 deg

In these studies, the Reynolds number at the blade tip, based on the tip chord and tip speed ΩR, is 3.9×10^6.

3.1 Power Generation at Zero Pitch

Figure 6 given below shows a comparison of generated power versus wind speed curves at zero-pitch condition using the BEM and CFD analysis both. A reasonable agreement is found both for the power production as a function of wind speed, and the coefficient of power as a function of tip speed ratio. It is also seen that the rated power of 2 MW is realized at the rated wind speed of 10 m/s. The variation of the coefficient of power with wind speed is also shown. The maximum value of the coefficient of power was 0.47 at the rated wind speed. This is slightly lower than the assumed value of 0.5 in the preliminary design, largely because the preliminary design process ignores a number of losses in the system including tip loses, non-uniform inflow effects, and swirl losses. At higher wind speeds above the rated wind speed of 10 m/s, the rotor stalls leading to a loss in the generated power. The blade element method does not account for the stall delay caused by centrifugal pumping effects, and gives rise to a somewhat steeper drop in power at high wind speeds.
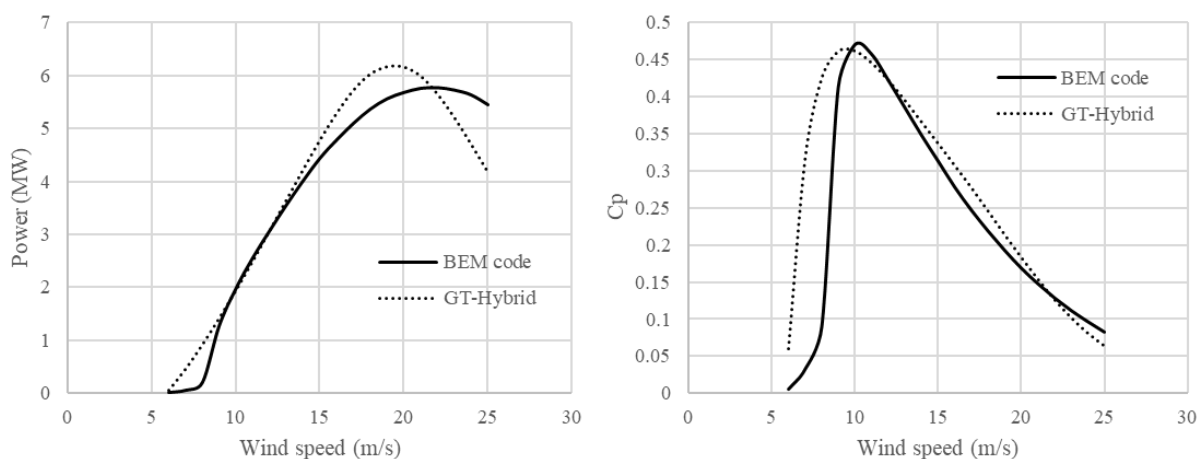

Fig. 6. Power and power coefficient versus wind speed curves at zero pitch

3.2 Power: Tip Speed Ratio and Pitch Angle Effects

The performance of the rotor at other conditions have also been modelled using the CFD analysis. Figure 7 shows the variation of the power coefficient versus tip speed ratio (TSR) for zero pitch, +2 degree pitch, and +4 degree pitch settings. It is seen that the proposed design has an optimum Cp value around 0.45 over a broad range of tip speed ratios and pitch settings, indicating that the rotor performs reasonably well even under off-design conditions.
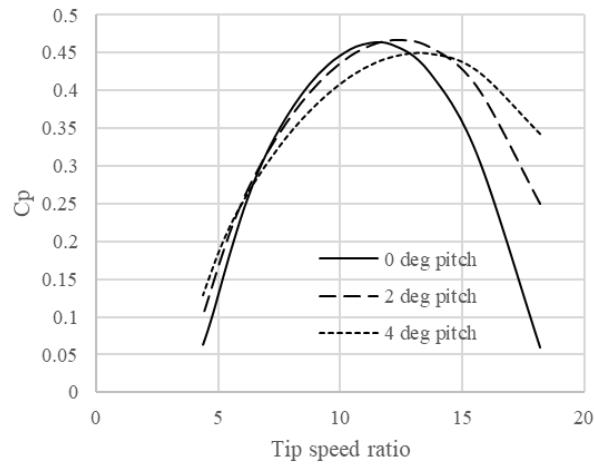
Fig. 7. Power coefficient versus wind speed at 0
deg, 2 deg, and 4 deg pitch

The rotor being analyzed was designed for zero pitch angle, and a tip speed ratio of 11. As seen in Figure 7, under this condition the maximum Cp is realized. It is also seen that a slightly higher rotor pitch value of 2 degrees further benefits the rotor performance in terms of maximum Cp value and power generation over a broad range of tip speed ratios between 10 and 15. The peak value of 0.45 is comparable to the power coefficient of existing 2 MW class wind turbines [30]. As the pitch setting increases to 4 degrees, the sectional angles of attack decrease, leading to a reduction in the propulsive sectional thrust forces in the plan of rotation. This leads to a reduction in torque and power production over much of the TSR range, except at very low TSR values (high wind conditions) when the rotor stalls.

3.3 Flow Visualization by CFD

CFD analysis is also an effective way of visualizing important flow phenomena and identifying key features of the flow.

3.3.1 Computed streamlines

Figure 8 below shows streamlines computed by GT-Hybrid at the rotor blade midspan and near the tip at rated wind speed and zero pitch.
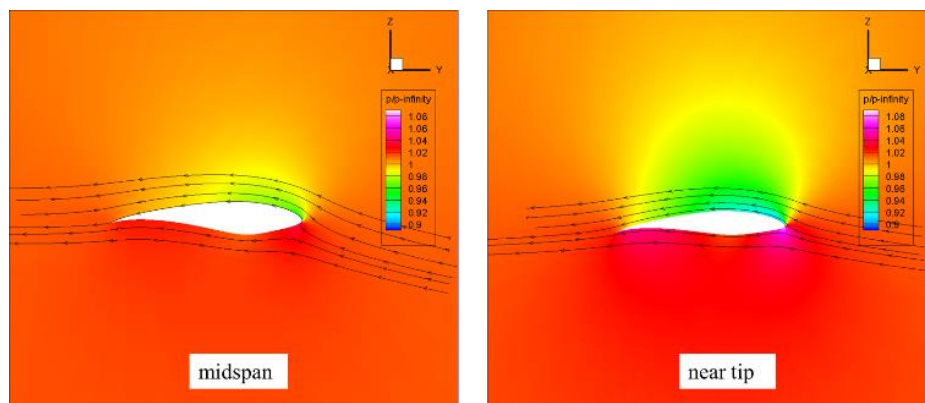

Fig. 8. Computed streamlines and pressure contour at rated wind speed and zero pitch

Figure 8 confirms that the proposed design, operating at the rated wind speed, has a fully attached flow over the entire span. At higher wind speeds, e.g. 25 m/s, there is extensive flow separation in the mid-span region as shown in Figure 9. Because of the blade twist, the tip region maintains attached flow over much of the airfoil section even at this extreme wind condition.
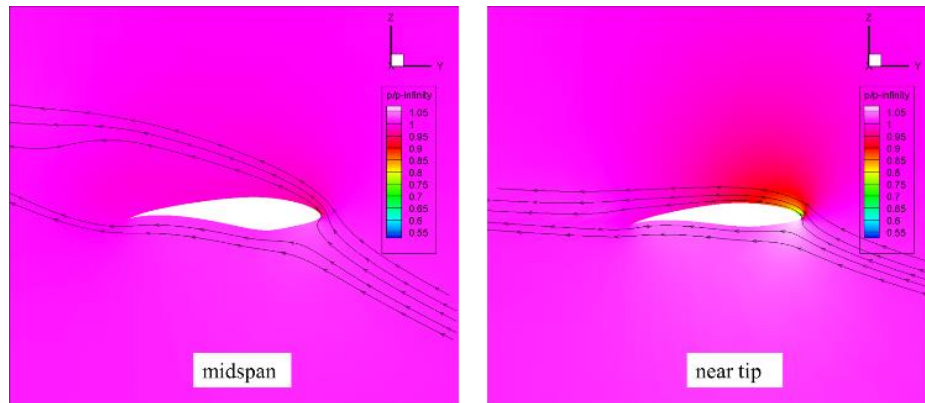

Fig. 9. Computed streamlines and pressure contour at wind speed of 25 m/s and zero pitch

The effects of blade pitch on the flow field, and consequently on the power coefficient may be analyzed. Figure 10 shows the computed streamlines and pressure contours of the rotor blade at 2 deg pitch in 9 m/s wind (TSR=12.13).
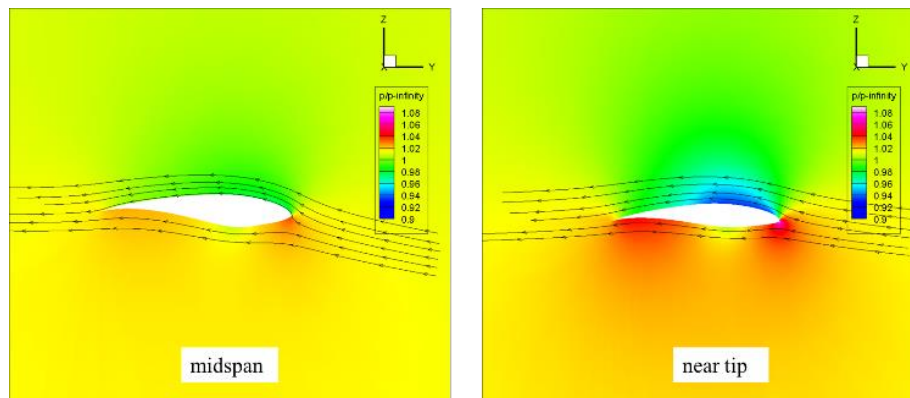

Fig. 10. Computed streamlines and pressure contour at wind speed of 9 m/s and 2 deg pitch

Comparing the pressure contours in Figure 10 to corresponding contours in Figure 8, it is clear that the region of suction pressure, i.e. the region where the gauge pressure is negative, on the upper surface of the rotor for the 2-degree pitch case is significantly larger than for its zero-pitch counterpart. This translates into higher lift force, and an increased thrust force along the plane of rotation. Consequently, an improvement in power coefficient is realized as seen in Figure 7.

4. Concluding Remarks

A wind turbine with a rated power of 2 MW at a rated wind speed of 10 m/s has been designed for a hypothetical offshore windfarm in the North Sea region. The design was based on aerodynamic considerations to meet design requirements. The performance of the turbine rotor under design conditions and off-design conditions has been analysed using the BEM theory and an in-house CFD

analysis. Results from the two techniques agree very well with each other for the power production and coefficient of power over a broad range of wind speeds, tip speed ratios, and blade pitch settings. The agreement is particularly good when flow field over the rotor is fully attached, as confirmed by flow visualization. At higher wind speed where flow separation is significant, a larger discrepancy between BEM and CFD results is observed. Although designed for zero pitch conditions at a tip speed ratio of 11, the rotor also per-formed well under off-design conditions.

In addition to aerodynamic performance studies, an industry standard model for rotor system cost and power production has been used to model he proposed windfarm, and this preliminary analysis indicates that the proposed system is economically viable.

Acknowledgement

References

[1] Butterfield, C. P., W. P. Musial, and D. A. Simms. *Combined experiment phase 1. Final report*. No. NREL/TP-257-4655. National Renewable Energy Lab., Golden, CO (United States), 1992.

[2] Simms, DAVID A., M. M. Hand, L. J. Fingersh, and D. W. Jager. *Unsteady aerodynamics experiment phases II-IV test configurations and available data campaigns*. No. NREL/TP-500-25950. National Renewable Energy Lab., Golden, CO (US), 1999.

[3] Hand, M. Maureen, D. A. Simms, L. J. Fingersh, D. W. Jager, and J. R. Cotrell. *Unsteady aerodynamics experiment phase V: test configuration and available data campaigns*. No. NREL/TP-500-29491. National Renewable Energy Lab., Golden, CO (US), 2001.

[4] Giguere, P., and M. S. Selig. *Design of a tapered and twisted blade for the NREL combined experiment rotor*. No. NREL/SR-500-26173. National Renewable Energy Lab., Golden, CO (US), 1999.

[5] Hand, M. M., D. A. Simms, L. J. Fingersh, D. W. Jager, J. R. Cotrell, S. Schreck, and S. M. Larwood. *Unsteady aerodynamics experiment phase VI: wind tunnel test configurations and available data campaigns*. No. NREL/TP-500-29955. National Renewable Energy Lab., Golden, CO.(US), 2001.

[6] Laino, D. J., and C. P. Butterfield. "Using YAWDYN to model turbines with aerodynamic control systems." *ASME SOL ENERGY DIV PUBL SED, ASME, NEW YORK, NY,(USA), 1994* 15 (1994): 27-30.

[7] Hansen, Martin OL. *Aerodynamics of wind turbines*. Routledge, 2000.

[8] Hansen, A. Craig, and D. J. Laino. "Users guide to the wind turbine dynamics computer programs YawDyn and AeroDyn for ADAMS." *Mechanical Engineering Department, University of Utah, Salt Lake City, Utah* 96, no. 22 (1996): 20.

[9] Sorensen, N., and M. Hansen. "Rotor performance predictions using a Navier-Stokes method." In *1998 ASME Wind Energy Symposium*, p. 25. 1998.

[10] Xu, Guanpeng, and Lakshmi N. Sankar. "Computational study of horizontal axis wind turbines." *Journal of solar energy engineering* 122, no. 1 (2000): 35-39.

[11] Benjanirat, Sarun. "Computational studies of the horizontal axis wind turbines in high wind speed condition using advanced turbulence models." PhD diss., Georgia Institute of Technology, 2006.

[12] Duque, Earl, C. Van Dam, and Shannon Hughes. "Navier-Stokes simulations of the NREL combined experiment phase II rotor." In *37th Aerospace Sciences Meeting and Exhibit*, p. 37. 1999.

[13] Sorensen, N. N., J. A. Michelsen, and S. Schreck. "Prediction of the NREL/NASA Ames wind tunnel test." *AIAA Paper* 31 (2002): 2002.

[14] Xu, Guanpeng, and Lakshmi Sankar. "Effects of transition, turbulence and yaw on the performance of horizontal axis wind turbines." In *2000 ASME Wind Energy Symposium*, p. 48. 2000.

[15] Sørensen, Niels N., J. A. Michelsen, and Scott Schreck. "Navier–Stokes predictions of the NREL phase VI rotor in the NASA Ames 80 ft× 120 ft wind tunnel." *Wind Energy: An International Journal for Progress and Applications in Wind Power Conversion Technology* 5, no. 2-3 (2002): 151-169.

[16] Benjanirat, Sarun, Lakshmi N. Sankar, and Guanpeng Xu. "Evaluation of turbulence models for the prediction of wind turbine aerodynamics." In *ASME 2003 wind energy symposium*, pp. 73-83. American Society of Mechanical Engineers Digital Collection, 2009.

[17]   Duque, E. P. N., M. D. Burkland, and W. Johnson. "Navier–Stokes and Comprehensive Performance Predictions of the NREL Phase IV Experiment. AIAA Paper 2003-0355." In *22nd ASME Wind Energy Symposium and the 41st AIAA Aerospace Sciences Meeting, Reno, NV*. 2003.
[18]   Madsen, Helge Aagaard, Niels N. Sørensen, and Scott Schreck. "Yaw aerodynamics analyzed with three codes in comparison with experiment." In *ASME 2003 Wind Energy Symposium*, pp. 94-103. American Society of Mechanical Engineers Digital Collection, 2009.
[19]   Benjanirat, Sarun. "Computational studies of the horizontal axis wind turbines in high wind speed condition using advanced turbulence models." PhD diss., Georgia Institute of Technology, 2006.
[20]   Benjanirat, Sarun, and Lakshmi Sankar. "Recent improvement to a combined Navier-Stokes/full potential methodology for modeling horizontal axis wind turbines." In *42nd AIAA Aerospace Sciences Meeting and Exhibit*, p. 830. 2004.
[21]   Tongchitpakdee, Chanin, Sarun Benjanirat, and Lakshmi N. Sankar. "Numerical simulation of the aerodynamics of horizontal axis wind turbines under yawed flow conditions." *Journal of solar energy engineering* 127, no. 4 (2005): 464-474.
[22]   Yu, D. O., and O. J. Kwon. "Time-accurate aeroelastic simulations of a wind turbine in yaw and shear using a coupled CFD-CSD method." In *Journal of Physics: Conference Series*, vol. 524, no. 1, p. 012046. IOP Publishing, 2014.
[23]   Becker, Max. "fastFoam-An aero-servo-elastic wind turbine simulation method based on CFD." Master's Thesis, Delft University, 2017.
[24]   Jonkman, Jason M., and Marshall L. Buhl Jr. "FAST user's guide." *National Renewable Energy Laboratory, Golden, CO, Technical Report No. NREL/EL-500-38230* (2005).
[25]   Zerbib, Nicolas, Andrew Heather Lassen Mebarek, and Marie Escouflaire. "Use OpenFoam coupled with the Finite Element Method suitable for Computational AeroAcoustics." In *proceedings, 4th OpenFoam Users Conference, Cologne, Germany*. 2016.
[26]   Popko, Wojciech, Matthias L. Huhn, Amy Robertson, Jason Jonkman, Fabian Wendt, Kolja Müller, Matthias Kretschmer et al. "Verification of a numerical model of the offshore wind turbine from the alpha ventus wind farm within oc5 phase iii." In *ASME 2018 37th International Conference on Ocean, Offshore and Arctic Engineering*. American Society of Mechanical Engineers Digital Collection, 2018.
[27]   Wijnant, I. L., G. J. Marseille, A. Stoffelen, H. W. van den Brink, and A. Stepek. "Validation of KNW atlas with scatterometer winds (Phase 3 of KNW project)." *KNMI, De Bilt, The Netherlands, Tech. Rep. TR-353* (2015).
[28]   Brand, A. J. "Offshore wind atlas of the Dutch part of the North sea." *China/Global Wind Power* (2008).
[29]   Geyer, Beate, Ralf Weisse, Peter Bisling, and Joerg Winterfeldt. "Climatology of North Sea wind energy derived from a model hindcast for 1958–2012." *Journal of Wind Engineering and Industrial Aerodynamics* 147 (2015): 18-29.
[30]   Malcolm, D. J., and A. C. Hansen. *WindPACT Turbine Rotor Design Study: June 2000--June 2002 (Revised)*. No. NREL/SR-500-32495. National Renewable Energy Lab.(NREL), Golden, CO (United States), 2006.
[31]   Tangler, James L., and Dan M. Somers. *NREL airfoil families for HAWTs*. No. NREL/TP-442-7109. National Renewable Energy Lab., Golden, CO (United States), 1995.
[32]   Fingersh, L., M. Hand, and A. Laxson. *Wind turbine design cost and scaling model*. No. NREL/TP-500-40566. National Renewable Energy Lab.(NREL), Golden, CO (United States), 2006.